Hemicyanine Dye as a Surfactant for the Synthesis of Bicontinuous Cubic Mesostructured Silica

Kun Hou,[†] Li Shen,[‡] Fuyou Li,*[,‡] Zuqiang Bian,[†] and Chunhui Huang*[,†,‡]

State Key Laboratory of Rare Earth Material Chemistry and Applications, Peking University, Beijing, 100871, P. R. China, and Laboratory of Advanced Materials, Fudan University, Shanghai, 200433, P. R. China.

Received: August 29, 2005; In Final Form: January 18, 2006

In this paper, we developed a facile way to synthesize highly ordered optically active MCM-48 at room temperature, by using mixtures of hemicyanine dye *N*-alkyl-2-[*p*-(*N*,*N*-diethylamino)-*o*-(alkyloxy)]pyridinium bromide (denoted as *o*-C_nPOC_m, Scheme 1) and cetyltrimethylammonium bromide (CTAB) as the structure-directing agents. The mesoporous materials were systematically characterized by powder X-ray diffraction, transmission electron microscopy, nitrogen sorption, and thermogravimetry. The resultant MCM-48 exibits unusually high thermal stability. For example, in the case of *o*-C_2POC_{14}, it can retain its cubic structure even under calcinations at 900 °C for 5 h, although the pore size is shifted to the micropore region because of shrinkage of the framework. The typical surface area and pore volume are 980 m^2/g and 0.44 cm^3/g, respectively, for the powder calcined under such a high temperature. This is the first report of room-temperature synthesis of MCM-48 with such good thermal stability using cationic−cationic mixed surfactant as the structure-directing agent. The fluorescence lifetimes of the as-synthesized mesostructured MCM-48 were also measured, and the result showed that the incorporated dye molecules have a 1 order of magnitude longer lifetime than that of free species in solution, showing that the hemicyanine dye molecules are well dispersed within the CTAB surfactant matrix. Furthermore, we compared eight other dye congeners (Scheme 1) to fully investigate the mesophase resulting from the dye−CTAB system. The results show that, upon addition of the dye surfactant to the starting mixtures, the mesostructured silica undergoes an intrinsic phase-transition process; however, specific dye geometry is required to obtain MCM-48 at room temperature. Those functionalities as well as the designed synthesis of this novel mesostructured MCM-48 material promise a bright future in multifunctional optical and electric nano- and microdevices (e.g., waveguides, laser, light-emitting diodes, etc.) and also shed light on the self-assembly behavior in complex colloidal system.

Introduction

The advent of ordered mesoporous materials in the early 1990s[1,2] stimulated intensive scientific activity and opened up exciting prospects in fields such as catalysis, chemical and biological separation, sensing, optoelectronics, and drug delivery, and for manufacturing advanced nanostructured materials.[3−11] The cationic long-chain quaternary ammonium surfactant cetyltrimethylammonium bromide (CTAB) was first used as the structure-directing agent to prepare the highly ordered materials.[1,2] Later, great efforts were made in the study of new surfactants, intending to prepare mesoporous materials with tailored properties. Anionic surfactants,[12−15] neutral amine surfactant,[16,17] gemini surfactants,[18,19] and nonionic poly(ethylene oxide) (PEO) surfactants[20,21] later demonstrated the possibilities of preparing mesoporous materials with various pore geometries and tunable pore size.

Among all the known mesophases of the M41S silica family first reported by Kresge et al.,[1,2] MCM-48 may be the most attractive one because of its unique pore structure. The MCM-48 material has been found to possess a bicontinuous mesostructure centered on the gyroid surface that divides the available pore system into an enantiomeric pair of subvolumes,[22,23] which is believed to be easier for the inclusion of various guest molecules in the cavum of the host materials compared to the more widely known hexagonally mesoporous silica, MCM-41. However, despite the merits of MCM-48, reports on the applications of the M41S materials have, until now, been severely biased to MCM-41. This bias may be attributed mostly to the fact that the synthesis of MCM-48 requires specific conditions. Initial studies of MCM-48 assembly indicated that the presence of ethanol as a cosurfactant was essential when using quaternary ammonium salts (e.g., CTAB) as the structure-directing agents.[24−27] Ethanol is believed to prevent the growth of the cylindrical micelles required for the synthesis of MCM-41.[28] Alternatively, it is also possible to prepare MCM-48 using other organic polar additives such as $(CH_3)_2NCH_2CH_2OH$ or $N(CH_2CH_2OH)_3$.[22] More recently, it was demonstrated that MCM-48 could be prepared from fumed silica and other silica sources without the use of organic additives.[29,30]

Mixed-surfactant systems exhibit very complex phase behavior in aqueous solution compared to single-surfactant systems[31,32] and have provided the ability to prepare high-quality mesoporous materials with different pore geometries. Ryoo and co-workers reported the synthesis of highly ordered MCM-48 with tunable pore size using cationic alkyltrimethylammonium bromide and neutral surfactant mixtures as the structure-directing agents.[32,33] MCM-48 can also be synthesized by cationic−anionic mixed surfactants.[34] However, until now, the cooperative

* Corresponding author. Tel: +86-10-62757156. Fax: +86-10-62757156. E-mail: chhuang@pku.edu.cn.
[†] Peking University.
[‡] Fudan University.

10.1021/jp054873x CCC: $33.50
Published on Web 04/25/2006

assembly of MCM-48 using cationic dye−cationic mixed surfactant is still left unexplored, which might be because the interplay between two cationic−cationic building blocks is less evident and hence less interesting than that of a cationic−anionic or ionic−nonionic system. Moreover, the geometrical importance of the cosurfactant on the resultant mesoporous materials has not been systematically studied before.

Hemicyanine dyes, which have both dyeing and amphiphilic properties, have been under substantial investigation in the past decades because of their possible applications in the fields of molecular electronics,[35] upconversion materials,[36] cell biology,[37] and photoelectroconversion.[38,39] While hemicyanine dye can be viewed as a cationic surfactant, it can lead to the synthesis of wormlike mesoporous silica alone.[40] The photophysical properties of the hemicyanine dyes are sensitive to the surroundings. However, the optical properties of hemicyanine dye trapped in mesoporous materials have seldom been reported.[6] Considering the multifunction of the hemicyanine dyes, it is of importance to study this system and hopefully shed some light on the optical properties of the dye molecules trapped in the mesostructured materials.

Here, we report an efficient synthesis route that can easily produce high-quality MCM-48 at room temperature. The whole synthetic procedure is quite simple and reproducible. The present method uses a hemicyanine dye−CTAB mixture as the structure-directing agent. The dyes (*o*-C_nPOC_m, where $n = 4, 3, 2$ and $m = 16, 14, 12$) are herein used as a surfactant. In this article, as an example, we first use one of the dyes (*o*-C_2POC_{14}) as a cosurfactant, together with CTAB, to synthesize and characterize highly ordered MCM-48 at room temperature. To further study this dye−CTAB mixed-surfactant system, eight other dye congeners were designed, synthesized, and employed to form mixed-surfactant systems, for comparison, to synthesize mesostructured silica. It is revealed that specific dye geometry is required to form MCM-48 at room temperature.

Experimental Section

Materials. The dye surfactants *o*-C_nPOC_m were prepared by a method reported earlier.[41] 2-Methylpyridine was quanterized with alkyl bromide of varied chain length and then condensed with a corresponding 4-diethylamino-2-alkyloxy- benzaldehyde. The diethylamino is used as the electron donor, while the alkyloxy hydrophobic tail is connected to the phenyl via an oxygen atom to increase the solubility of the hemicyanine dye. ^{1}H NMR, elemental analyses, and electrospray ionization mass spectrometry (ESI-MS) results showed that all the dye molecules were successfully synthesized (See Supporting Information for details). The other chemicals used in the experiments were purchased from Beijing Chemical Factory and used without further purification.

Synthesis of Mesoporous Silica. In a typical synthesis procedure, a certain amount of *o*-C_2POC_{14} and 0.6 g of CTAB were mixed in 25 g of deionized water and 15 g of concentrated $NH_3{\cdot}H_2O$ (28%). The mixture was first heated to about 40 °C to dissolve the surfactant mixture completely. Then tetraethyl orthosilicate (TEOS) was added to the mixture following its cooling to room temperature. The composition of the mixtures is expressed in mole ratio as 1 CTAB/*x* TEOS/*y* *o*-C_2POC_{14}/1208 H_2O/150 NH_3. After stirring for 4 h at room temperature, filtration allowed for the separation of the products as a yellow precipitate, which was washed with water and dried in a vacuum at room temperature. The surfactants were mostly removed by calcination at 600 °C for 5 h in air. It should be noted here that hydrothermal treatment is not needed in the experiments. For comparison, a dye-free MCM-41 sample was synthesized from the starting mixture of 1 CTAB/9.2 TEOS/1208 H_2O/150 NH_3.

In the control experiments for all of the dye congeners, the CTAB/TEOS ratio was kept constant, while only different amounts of the respective hemicyanine dye were added to get gels with the following composition: 1 CTAB/9.2 TEOS/*y* *o*-C_nPOC_m/1208 H_2O/150 NH_3.

Characterization. Powder X-ray diffraction (XRD) was conducted with a Rigaku D/ MAX 2000 diffractometer using Ni-filtered Cu Kα radiation operated at 40 KV and 100 mA, with a scan rate of 1°/min and a step of 0.02°. Nitrogen adsorption/desorption isotherms were performed at 77 K using an ASAP 2010 analyzer (Micrometrics, Co. Ltd.). The samples were first degassed at 200 °C to a residue pressure below 10 μm Hg. The surface area was calculated using the Brunauer−Emmett−Teller (BET) method from the adsorption data obtained in a relative pressure (P/P_0) range of 0.05−0.25, and the pore size distribution (PSD) was evaluated from the adsorption branch of the isotherm based on the Barrett−Joyner−Halenda (BJH) method. The pore volume was estimated from the single point at a relative pressure of $P/P_0 = 0.99$, assuming that the nitrogen adsorption on the external surface was negligible compared to the adsorption in the pores. Weight-change curves were recorded on an SDT 2960 simultaneous DTA-TGA instrument with a heating rate of 10 °C/min. Transmission electron microscope (TEM) images were taken on a JEOL 2011 microscope operated with an accelerated voltage of 200 kV. The sample was dispersed in acetone and deposited on a carbon grid. ^{1}H NMR spectra were recorded on a Bruker 400 MHz spectrometer. Elemental analyses were performed on an Elementar Vario EL instrument. ESI-MS spectra were obtained by using a Finnigan LCQ Deca XP Plus ion trap mass spectrometer. The fluorescence lifetime measurement was carried out with an Edinburgh LifeSpec-ps spectrometer.

Results and Discussion

MCM-48 Synthesized From *o*-C_2POC_{14}−CTAB Mixed Surfactants. For clarity, the dye *o*-C_2POC_{14} will be taken as an example to discuss the synthesis, structure, morphology, thermal stability, and formation conditions of MCM-48 in the system of mixed surfactants. The lifetimes of the dye trapped in the as-synthesized MCM-48 were also studied.

XRD Measurement. Figure 1 shows the XRD patterns of the synthesized mesoporous silica at room temperature from the starting composition of 1 CTAB/9.2 TEOS/0.5 *o*-C_2POC_{14}/1208 H_2O/150 NH_3. As can be seen from the figure, two diffraction peaks of the as-synthesized product can be clearly seen at $2\theta = 2.16°$ and 2.49° with *d* values of 4.09 and 3.55 nm, respectively. These peaks can be indexed as the (211) and (220) diffraction peaks, which belong to a bicontinuous cubic space group (*Ia*3*d*) symmetry. After calcinations at 600 °C for 5 h, the diffraction peaks become more resolved, and six peaks can be clearly observed in the 2θ ranging from 3 to 6°, which can be indexed to the (321), (400), (420), (332), (442), and (431) reflections, confirming the existence of a high-quality *Ia*3*d* mesophase, namely MCM-48. The unit cell parameters of the as-synthesized and calcined cubic mesophase, calculated by the formula $a = d_{211}(h^2+k^2+l^2)^{1/2}$, are 10.01 and 9.24 nm, respectively.

TEM Analysis. Figure 2 shows the representative TEM images of the calcined mesoporous silica (600 °C, 5 h) prepared with an *o*-C_2POC_{14} and CTAB mixed-surfactant system at room temperature. The (111) and (311) projection planes (Figure 2) and other images clearly show the presence of a highly ordered *Ia*3*d* cubic mesophase.

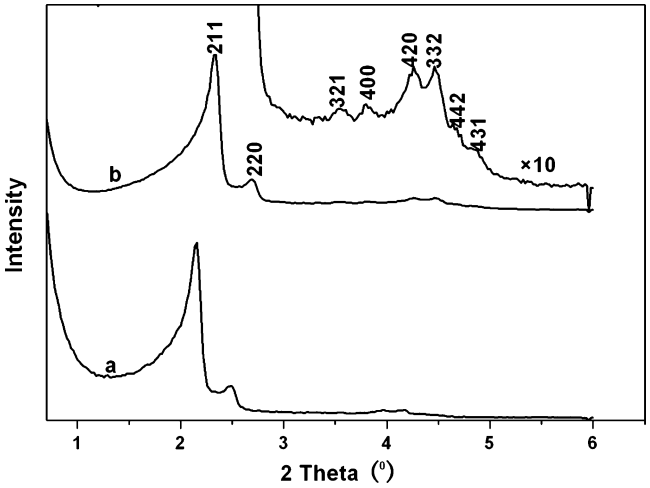

Figure 1. XRD patterns of the mesoporous silica prepared from the starting mixture of 1 CTAB/9.2 TEOS/0.5 *o*-C_2POC_{14}/1208 H_2O/150 NH_3 at room temperature (a) as-synthesized and (b) calcined at 600 °C for 5 h.

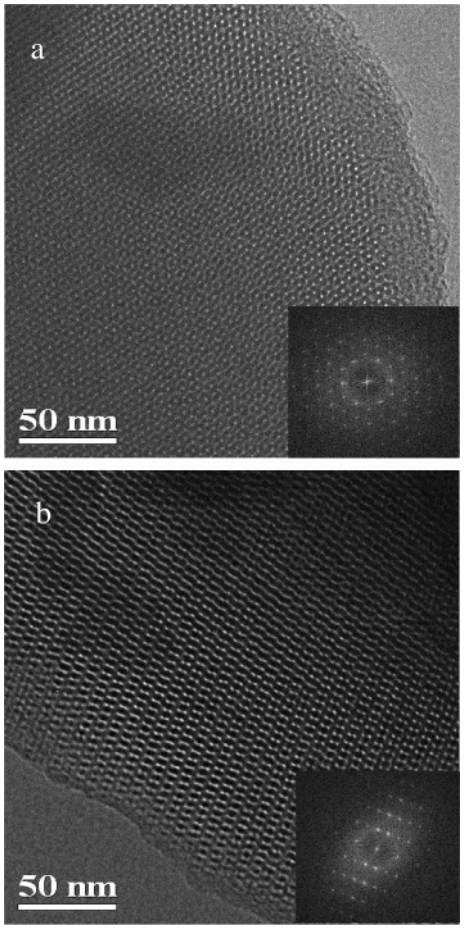

Figure 2. TEM images and the corresponding Fourier diffractograms of the calcined mesoporous silica prepared from the starting mixture of 1 CTAB/9.2 TEOS/0.5 *o*-C_2POC_{14}/1208 H_2O/150 NH_3 at room temperature, viewed from the (a) [111] and (b) [311] directions.

Nitrogen Adsorption−Desorption Measurement. Nitrogen adsorption isotherms for the MCM-48 calcined at 600 °C for 5 h are shown by curve a in Figure 3. The isotherms exhibit a sharp step in the relative pressure range $P/P_0 = 0.30-0.40$, which is associated with capillary condensation in the channels of MCM-48. The sharpness of the capillary condensation step indicates the uniformity of the pore channels and their narrow size distribution. The capillary condensation is clearly accompanied by adsorption−desorption hysteresis, which is observed at the relative pressure 0.35−0.40. The BJH pore diameter, BET surface area, and pore volume of the calcined sample are 2.50 nm, 1134 m^2/g, and 1.00 cm^3/g, respectively. The results clearly show that the MCM-48 material obtained at room temperature has a well-defined porous structure and a uniform pore structure, which were already confirmed by TEM analysis.

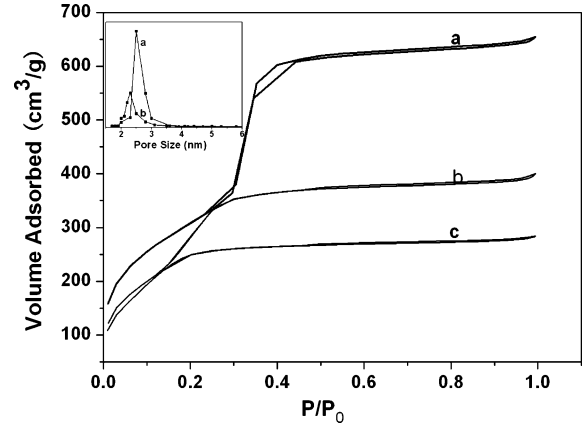

Figure 3. Nitrogen adsorption−desorption isotherms and PSD curves (inset) for the calcined MCM-48 prepared from the starting mixture of 1 CTAB/9.2 TEOS/0.5*o*-C_2POC_{14}/1208 H_2O/150 NH_3 at room temperature and calcined at (a) 600 °C for 5 h, (b) 800 °C for 5 h, and (c) 900 °C for 5 h.

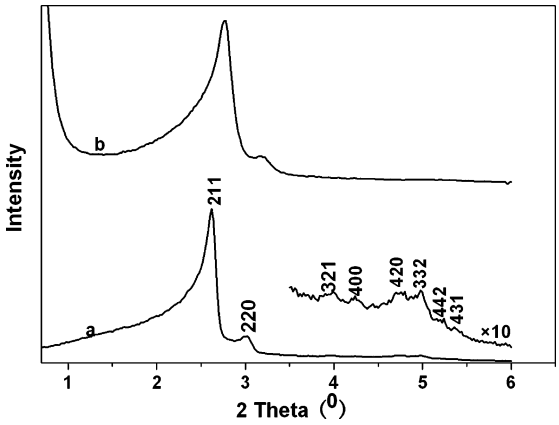

Figure 4. XRD patterns of MCM-48 calcined at higher temperatures for 5 h at (a) 800 °C and (b) 900 °C.

Thermal Stability. The thermal stability of the obtained MCM-48 was investigated by subjecting the material to calcinations at high temperatures. The XRD patterns of the material calcined at high temperatures are displayed in Figure 4. Representatively, MCM-48 herein can retain its long-range order upon calcination at 800 °C for 5 h: the (321), (400), (420), (332), (442), and (431) diffraction peaks are still well preserved at this temperature. The N_2 adsorption−desorption isotherms are of type IV at this temperature, indicating that the pore size of the resulting sample is in the mesoporous region (curve b in Figure 3). Compared with the sample calcined at 600 °C for 5 h, the shrinkage in cell parameter is about 12% for the sample calcined at 800 °C. The pore size, BET surface area, and pore volume for the sample are 2.30 nm, 1111 m^2/g, 0.62 cm^3/g, respectively (Table 1). When the MCM-48 was treated at 900 °C for 5 h, it still retained its cubic mesostructure, as evidenced by the presence of the (211) and (220) diffraction peaks. At this temperature, the cell parameter for the sample is 7.80 nm, about 19% in shrinkage compared with that calcined at 600 °C for 5

TABLE 1: Effect of Calcination Temperature on the Pore Structure of MCM-48

sample[a]	d_{211} (nm)	a (nm)	S_{BET} (m^2/g)	pore size (nm)	pore volume (cm^3/g)
1b	3.77	9.24	1134	2.50	1.00
4a	3.37	8.25	1111	2.30	0.62
4b	3.17	7.78	980	*b*	0.44

[a] 1b, 4a, and 4b refer to the samples shown in curve b of Figure 1, and curves a and b of Figure 4, respectively. [b] The pore size is less than 2 nm.

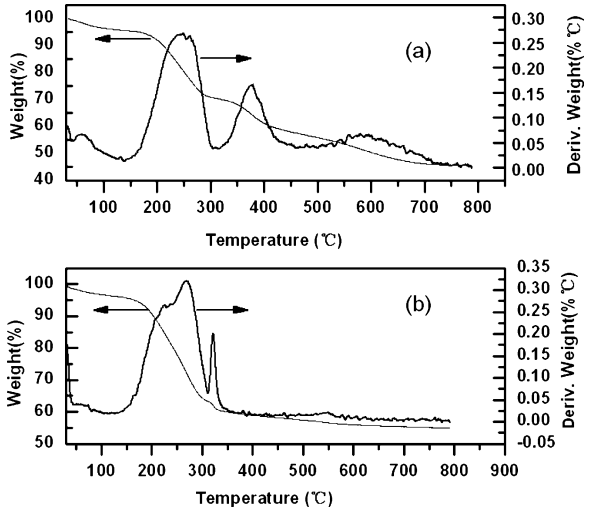

Figure 5. Thermogravimetry analysis curves of (a) as-synthesized MCM-48 prepared from the starting mixture of 1 CTAB/9.2 TEOS/0.5*o*-C_2POC_{14}/1208 H_2O/150 NH_3 at room temperature and (b) MCM-41 prepared from the starting mixture of 1 CTAB/9.2 TEOS/1208 H_2O/150 NH_3 at room temperature.

h. The N_2 adsorption−desorption isotherms for this sample (curve c in Figure 3) are type I, showing that the pore size is in the microporous region because of the shrinkage of the framework under high-temperature treatment. The BET surface area and pore volume are shown in Table 1. As seen from the table, the BET surface area for this sample remains very high (980 m^2/g), showing that the porous structure is not damaged at such a high temperature. It has been reported that the pore structure of pure silica MCM-48 material prepared from TEOS completely collapses upon calcination at 750 °C, being demonstrated by the disappearance of the capillary condensation step in the N_2 isotherm and the diffraction lines of the XRD pattern.[42] However, the synthesized MCM-48 at room-temperature herein is very stable, even under calcinations at 900 °C for 5 h. Pang et al. reported that the mesoporous silica with *Ia*3*d* cubic structure prepared using CTAB−sugar mixed templates is stable under a calcination temperature of 900 °C for 4 h; however, the mesostructured silica was calcined under the protection of N_2. The carbon transformed from the sugar surfactant contributes to the thermal stability of the MCM-48 mesostructure. The structure of the as-synthesized powders is completely destroyed when calcined in air at 900 °C for 4 h.[43] Figure 5a shows the thermogravimetric weight-change curve (TG) and the weight-change derivative (DTA) curve of the as-synthesized MCM-48. Four major weight loss regions can be clearly observed. The weight loss below 130 °C can be attributed to the thermodesorption of physically adsorbed water (about 4 wt %).[33,44] Compared with the TG-DTA curve of the alkyltrimethylammonium-directed MCM-41 (Figure 5b), the second weight loss between 130 and 325 °C can be attributed mainly to the decomposition of the alkyltrimethylammonium surfactant.[33] The two weight losses between 325 and 700 °C are too large to be attributed solely to the releasing of water via condensation of the silanol.[33,44a] Therefore, these two weight losses (about 23 wt %) for the MCM-48 material can be assigned to the decomposition of the dye surfactant. From the above results, one can also see that the full decomposition of the dye surfactant occurs at a relatively higher temperature compared with that of CTAB. The ultrahigh thermal stability of the MCM-48 material may be due to the higher decomposition temperature of the dye surfactants compared to CTAB, thus the more stable dye surfactant could partially protect the SiO_2 mesophase from collapse and make it more condensed before organic templates are totally removed.

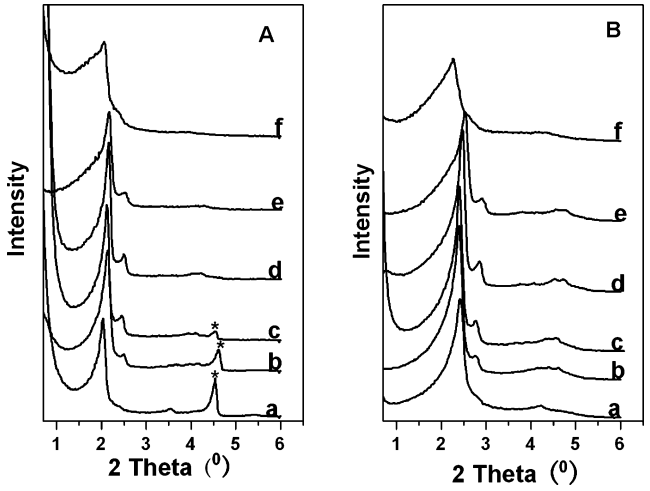

Figure 6. XRD patterns of the mesoporous silica synthesized with 1 CTAB/*x* TEOS/0.5 *o*-C_2POC_{14}/1208 H_2O/150 NH_3 (A) as-synthesized and (B) calcined at 600 °C for 5 h with (a) $x = 4.3$, (b) $x = 5.3$, (c) $x = 7.3$, (d) $x = 8.0$, (e) $x = 10.6$, and (f) $x = 11.2$. The peaks marked by asterisks (∗) are from the lamellar mesophase.

The Effect of the TEOS Amount (x) on the Pore Structure of the Mesoporous Materials. The effects of the TEOS-to-CTAB molar ratio (TEOS/CTAB, *x*) on the resultant mesostructure of the mesoporous materials are shown in Figure 6. Given that the amount of *o*-C_2POC_{14} is fixed at 0.5, when the molar ratio of TEOS to CTAB is 4.3, that is, the composition of the starting mixture corresponds to 1 CTAB/4.3 TEOS/0.5 *o*-C_2POC_{14}/1208 H_2O/150 NH_3, an intense peak can be seen at the 2θ value of 4.53°, which might indicate the formation of a lamellar mesophase. The disappearance of this peak after calcinations further corroborates this speculation. This result shows that only mixed mesophase is obtained in the system. A weak (211) diffraction peak of MCM-48 is observed on the calcined XRD pattern, but the dominant phase is hexagonal mesophase judged from the calcined XRD pattern. This fact reflects that the mixed mesophase obtained at this ratio of starting mixture is composed of *p*6*m*, *Ia*3*d*, and lamellar mesophase. When the *x* ratio is increased to 5.3, the peak located at 4.53° becomes much weaker, while another peak, which can be indexed as the (211) diffraction of the cubic *Ia*3*d* mesophase, becomes clearly discernible at a 2θ value of 2.50°. This fact suggests that the MCM-48 mesophase begin to be the dominant mesophase at this *x* ratio. After calcination, the XRD pattern can only be indexed as the *Ia*3*d* space group. When the *x* ratio is further increased to 7.3, the peak that belongs to the lamellar phase becomes even weaker, and the (211) peak becomes more intense, which reveals that the lamellar phase becomes smaller with an increase in the amount of TEOS. The calcined XRD pattern shows the existence of a high-quality *Ia*3*d* mesophase with several other diffraction peaks clearly distinguishable at

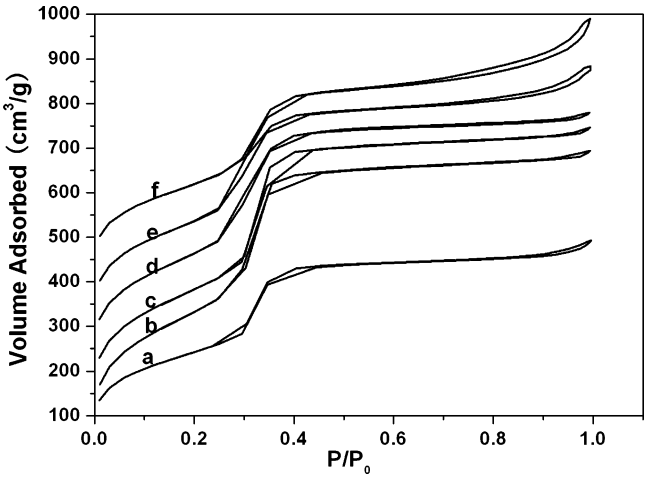

Figure 7. N_2 adsorption−desorption isotherms of the calcined (600 °C for 5 h) mesoporous silicas synthesized from 1 CTAB/*x* TEOS/0.5 *o*-C_2POC_{14}/1208 H_2O/150 NH_3 with (a) $x = 4.3$, (b) $x = 5.3$, (c) $x = 7.3$, (d) $x = 8.0$, (e) $x = 10.6$, and (f) $x = 11.2$.

TABLE 2: Properties of the Mesoporous Silicas Obtained with Different TEOS-to-CTAB Ratios (*x* Value)

x value	S_{BET} (m^2/g)	pore size (nm)	pore volume (cm^3/g)
4.3	881	2.50	0.76
5.3	1228	2.49	1.07
7.3	1163	2.50	1.05
8.0	1146	2.50	1.01
10.6	1025	2.49	0.97
11.2	907	2.60	0.95

the 2θ range of 3−6°. When the *x* ratio reaches 8.0, the lamellar phase totally disappears, and only a pure cubic *Ia*3*d* mesophase exists, as shown by curves d in Figure 6. The *Ia*3*d* symmetry can be maintained when the *x* value is increased to 10.6. Products with disordered mesostructure are formed when the *x* is increased to 11.2, as indicated by the broad diffraction peak. All the above results suggest that the bicontinuous cubic mesophase can only be prepared in a very narrow TEOS-to-CTAB ratio range with an *x* value between 8.0 and 10.6. It should be noted here that the mesostructure of the silica transformed from a *p*6*m* and lamellar mesophase to an *Ia*3*d* mesophase with increasing the amount of TEOS in the system.

To further investigate the pore structure of the calcined mesoporous materials formed with different TEOS/CTAB ratios, the nitrogen adsorption−desorption isotherms are shown in Figure 7. As can be seen from the figure, the isotherms of the different silica are all of type IV with capillary condensation at the relative pressure between 0.25 and 0.40. The most probable pore size, BET surface area, and total pore volumes are listed in Table 2. The pore diameter, surface area, and the pore volume of the sample obtained with $x = 4.3$ are 2.50 nm, 881 m^2/g, and 0.76 cm^3/g, respectively.

Effect of the Molar Ratio of Dye to CTAB (y) on the Mesostructure of Silica. Figure 8 represents the XRD patterns for the different silica mesophases obtained with an increasing amount of *o*-C_2POC_{14} molecules in the system of 1 CTAB/9.2 TEOS/*y* *o*-C_2POC_{14}/1208 H_2O/150 NH_3. From the XRD patterns, it is clear that, without any addition of the dye surfactant, the synthesized material is typically MCM-41. The long-range order of the material is evidenced by a strong diffraction peak at $2\theta = 2.21°$ and two other distinguishable peaks between 3 and 5°, which can be attributed to the (110) and (200) diffraction peaks. Normally, excessive dye molecule doping might degrade the order of the mesostructure of the obtained mesoporous

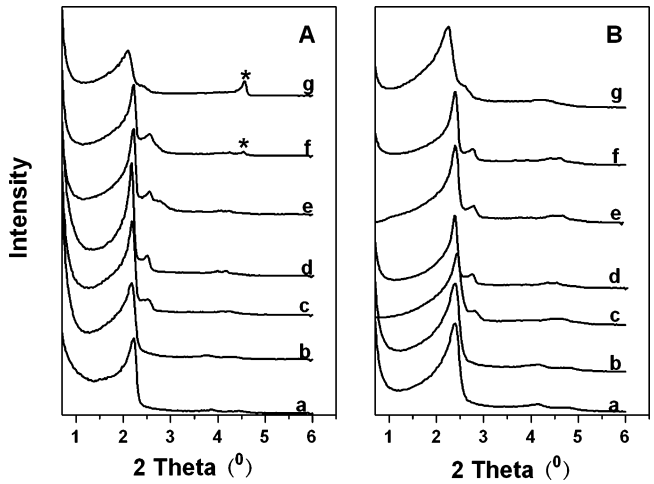

Figure 8. XRD patterns of the mesoporous silica (A) as-synthesized and (B) calcined at 600 °C for 5 h, synthesized from 1 CTAB/9.2 TEOS/*y* *o*-C_2POC_{14}/1208 H_2O/150 NH_3 with (a) $y = 0$, (b) $y = 0.3$, (c) $y = 0.4$, (d) $y = 0.6$, (e) $y = 0.7$, (f) $y = 0.9$, and (g) $y = 1.2$. The peaks marked by asterisks (∗) are from the lamellar mesophase.

materials.[45] However, as can be seen from the figure, the hexagonal symmetry of the hybrid material is still well preserved, even when the dye amount *y* is increased to 0.3. More interestingly, when the dye surfactant amount *y* is increased to 0.4, the phase of the mesostructure starts to transform from hexagonal *p*6*m* (MCM-41) to a bicontinuous three-dimensional cubic *Ia*3*d* mesophase (MCM-48). A highly ordered pure *Ia*3*d* cubic mesophase can be easily obtained in the *y* range of 0.4−0.6. Increasing the added dye surfactant amount to $y = 0.7$, the (220) diffraction peak is greatly widened, indicating that the cubic mesophase is contaminated by another mesophase. However, after calcinations, the XRD pattern shows a well-ordered pure *Ia*3*d* mesophase, suggesting the existence of a mixed mesophase consisting of MCM-48 and a lamellar phase with MCM-48 being the dominant phase in the as-synthesized materials. When the *y* value is increased to 1.2, another peak is clearly observed at $2\theta = 4.54°$, which clearly indicates the formation of a lamellar mesophase. After calcinations, the remaining signal points toward the existence of a less-ordered cubic *Ia*3*d* structure, which shows that the *Ia*3*d* mesostructure is not totally transformed to the lamellar phase with the increasing addition of the dye surfactant. Further increase of the dye amount leads to the insolubility of the mixed surfactant at room temperature, and thus no pure lamellar phase is obtained at the present stage.

The Fluorescence Property of the Dye Molecules Trapped in the As-Synthesized MCM-48. Figure 9 shows the fluorescence decay curves of the as-synthesized MCM-48 from the starting mixtures of 1 CTAB/9.2 TEOS/0.5 *o*-C_2POC_{14}/1208 H_2O/150 NH_3 and the dye in chloroform solution. Here, 10^{-4} M dye chloroform solution was chosen for comparison. As can be seen from the figure, both of the decay curves obey multiexponential kinetics. The fluorescence lifetimes of the dye in the as-synthesized MCM-48 are 5.25 (22.56%), 1.60 (50.38%) and 0.43 ns (27.06%), while those for the dye chloroform solution are 0.58 (15.73%) and 0.13 ns (84.27%). The average lifetime-($<\tau> = \alpha_1\tau_1 + \alpha_2\tau_2 + \alpha_3\tau_3$) for the dye in MCM-48 is 2.10 ns, which is a an order of magnitude longer than the 0.20 ns lifetime for dye in chloroform solution. This result is quite interesting, especially in the high doping ratio of the dye (dye/CTAB = 1/2, molar ratio). The photophysics of hemicyanine dye is very sensitive to the surroundings. It is considered that the twisted intramolecular charge-transfer (TICT) state of

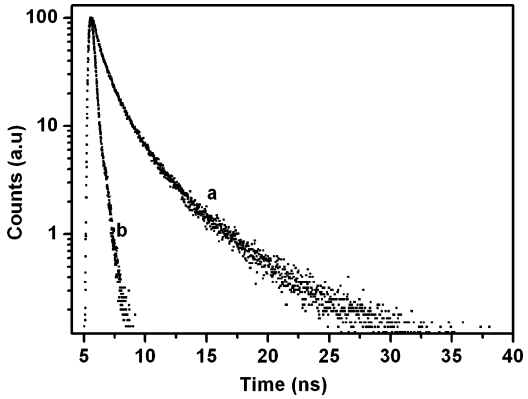

Figure 9. The fluorescence decay curves of (a) hybrid MCM-48 from the starting mixture of 1 CTAB/9.2 TEOS/0.5 *o*-C_2POC_{14}/1208 H_2O/ 150 NH_3 and (b) a dye chloroform solution of 10^{-4} M.

hemicyanine dye is a nonradiative state, which is also the most efficient deactivation process of the excited state of hemicyanine.[46] According to the TICT model, the excited dye molecules initially form a moderately polar state with a geometry similar to that in the ground state. Subsequently, these excited molecules undergo an intramolecular transfer of an electron from a donor to an acceptor, which is accompanied by a twist around the bond joining the donor and the acceptor. [47] It is intuitive to suppose that, if the hemicyanine dyes are confined by some external force to prevent the formation of the TICT state, the lifetime as well as the fluorescence quantum yield will be enhanced. The incorporated dye molecules are confined in the mesostructured silica, so it is reasonable that the fluorescence lifetimes of the incorporated dyes should be much longer than that in solution. However, if hemicyanine dye is used as surfactant alone, the lifetimes of the hemicyanine dye trapped in the wormlike mesostructured silica are much shorter than those of the dye trapped in the present MCM-48 material because of the fluorescence self-annihilation effect among the dye aggregates despite the blocking of the TICT state.[40] This result indicates that, aside from the blocking of the TICT states, there is another reason that also contributes to the prolonging of the fluorescence lifetime of the trapped dye molecules. Because of the peculiar amphiphilic property of the hemicyanine dye, mixed micelles are formed between the dye molecules and the CTAB molecules, and thus the dye molecules are well dispersed within the CTAB surfactant matrix. The good dispersion of the dye molecules by the CTAB molecules helps to avoid the self-annihilation of the dye molecules. Because of the aforementioned reasons, the lifetimes of the dye molecules are much longer than those in chloroform solution, even if the doping ratio of the dye is very high. This character makes this novel dye-doped mesostructured silica quite attractive for applications as laser or waveguide media.[6]

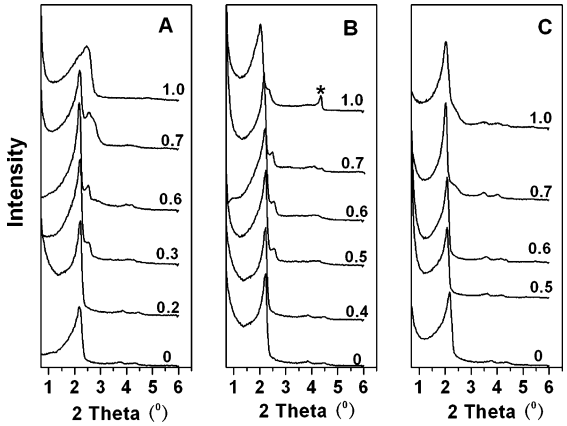

Figure 10. XRD patterns of the mesophases formed using 1 CTAB/ 9.2 TEOS/*y* *o*-C_nPOC_{16}/1208 H_2O/150 NH_3 with the dye molecules (A) *o*-C_4POC_{16}, (B) *o*-C_3POC_{16}, and (C) *o*-C_2POC_{16}. The amounts of the dye (*y*) added to the starting mixture are labeled on the XRD curves. The peak marked by asterisk (*) in panel B is from the lamellar mesophase.

The Influence of the Geometrical Factors of the Dyes on the Mesostructure. Previous reports in the literature have documented well that the structures of the polar additives have a great effect on the phase behavior of the silicate−surfactant systems.[48] However, in the present system with two cationic mixed surfactants as the structure-directing agent, the systems and the structure of the dyes are more complicated. To understand how the geometrical factors of the dyes effect the mesostructure of the resultant mesostructured materials, a comparison of nine dye congeners (Scheme 1) was carried out under similar conditions in the system of 1 CTAB/ 9.2 TEOS/ *y* *o*-C_nPOC_m/ 1208 H_2O/ 150 NH_3. Figures 10, 11, and 12 show the respective silica mesophase transitions upon addition of one of the other eight dyes. From the figures and Table 3, one can see that not all the hemicyanine dyes are able to facilitate the synthesis of MCM-48 at room temperature.

o-C_nPOC_{16} as Cosurfactant. When the alkyloxy group long hydrophobic tails are fixed as cetyl (Figure 10), we can see that the hydrophilic head, namely, the volume of the polar head of the dye surfactant, plays important roles in determining the pore structures of the resultant mesoporous materials with the addition of the dye molecules. For *o*-C_4POC_{16}, MCM-41 begins to transform to MCM-48 at the *y* value of 0.3, but this value is increased to 0.5 when the alkyl of the polar head is changed from butyl to propyl. MCM-48 material cannot be efficiently obtained when the alkyl of the hydrophilic head is further changed from propyl to ethyl, and only a mixed mesophase of MCM-41 and MCM-48 is obtained, even when the *y* value is increased to 1.0. This result shows that dye addition also changes

SCHEME 1. Structure of the Hemicyanine Dye Congeners Used in the Experiments

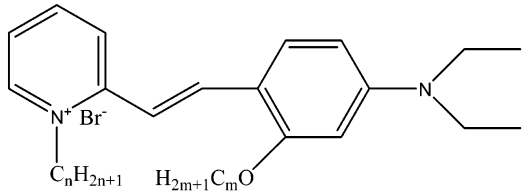

When m=16 (a_1) n= 4, *o*-C_4POC_{16}; (a_2) n= 3, *o*-C_3POC_{16}; (a_3) n= 2, *o*-C_2POC_{16};

m=14 (b_1) n=4, *o*-C_4POC_{14}; (b_2) n= 3, *o*-C_3POC_{14}; (b_3) n= 2, *o*-C_2POC_{14};

m=12 (c_1) n=4, *o*-C_4POC_{12}; (c_2) n= 3, *o*-C_3POC_{12}; (c_3) n= 2, *o*-C_2POC_{12};

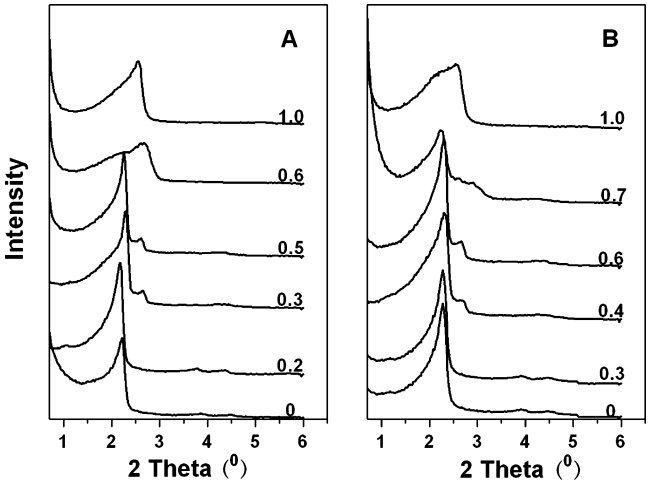

Figure 11. XRD patterns of the mesophases formed using 1 CTAB/9.2 TEOS/*y* *o*-C_nPOC_{14}/1208 H_2O/150 NH_3 with the dye molecules (A) *o*-C_4POC_{14} and (B) *o*-C_3POC_{14}. The amounts of the dye (*y*) added to the starting mixture are labeled on the XRD curves.

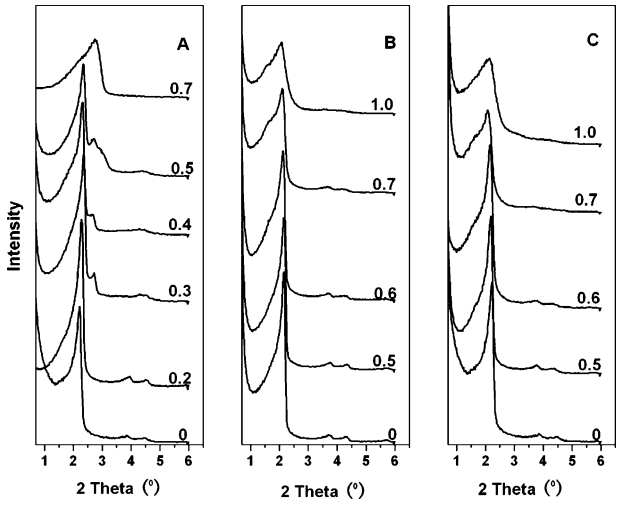

Figure 12. XRD patterns of the mesophases formed using 1 CTAB/9.2 TEOS/*y* *o*-C_nPOC_{12}/1208 H_2O/150 NH_3 with the dye molecules (A) *o*-C_4POC_{12}, (B) *o*-C_3POC_{12}, and (C) *o*-C_2POC_{12}. The amounts of the dye added to the starting mixture are labeled on the XRD curves.

TABLE 3: Influence of the Geometrical Factors of the Dyes on the Ratio of *o*-C_nPOC_m/CTAB (*y*), Which Is Essentially Needed for the Formation of MCM-48 in the Mixed-Surfactant System of 1 CTAB/9.2 TEOS/*y* *o*-C_nPOC_m/1208 H_2O/150 NH_3

n/*y*/*m*[a]	16	14	12
4	0.3−0.6	0.3−0.5	0.3−0.4
3	0.5−0.7	0.4−0.6	*b*
2	*b*	0.4−0.6	*b*

[a] The formula of the hemicyanine dye molecules is denoted as *o*-C_nPOC_m, where $n = 4, 3, 2$; $m = 16, 14, 12$. [b] Pure MCM-48 cannot be obtained.

micelle curvature, but the appropriate value to synthesize pure MCM-48 is not obtained.

o-C_nPOC_{14} as Cosurfactant. When the alkyloxy hydrophobic long tails are fixed to tetradecyl, the influence of the alkyl hydrophilic head on the phase behavior of the mixed surfactant is completely different (Figure 11) compared to that of *o*-C_n-POC_{16}. For *o*-C_4POC_{14}, MCM-48 can be obtained when the *y* value is increased to 0.3, as is the case for *o*-C_4POC_{16}. But, in Figure 11B, the sufficient dye amount for the phase transformation decreases from $y = 0.5$ in Figure 10B to $y = 0.4$, which proves that the long alkyl hydrophobic tails also play an important role in determining the behavior of the mixed surfactant. This conclusion is further verified by Figure 8A. High-quality MCM-48 still can be obtained with the addition of the ethyl-headed *o*-C_2POC_{14}, as demonstrated in the above part of this article, whereas *o*-C_2POC_{16} is proved to be invalid for the synthesis of pure MCM-48, as shown in Figure 10C. In Figure 8A, MCM-48 emerges as the *y* value is increased to 0.4, as is the case for *o*-C_3POC_{14}.

o-C_nPOC_{12} as Cosurfactant. When the alkyloxy long tails of dyes are further shortened from tetradecyl to dodecyl to form dye *o*-C_4POC_{12}, *o*-C_3POC_{12}, and *o*-C_2POC_{12}, the mixed-surfactant behavior is further changed. In Figure 12A, we can see that the *Ia*3*d* mesophase can be formed in a much narrower *y* range of 0.3−0.4, and the cubic mesophase begins to be contaminated by disordered materials when the *y* value is further increased to 0.5, as evidenced by the broadening of the (211) diffraction peak. When the alkyl group hydrophilic head is changed from butyl to propyl (*o*-C_3POC_{12}), as the XRD pattern shows in Figure 12B, MCM-48 cannot be formed, even when the *y* value is enhanced to 0.6. The *p*6*m* mesostructure is degraded when the *y* value is further increased to 0.7, as proved by the widened (100) diffraction peak. Products with disordered structure that cannot be indexed to any space group are formed, as indicated by the broad XRD diffraction peak when the *y* value is increased to 1.0. The case for *o*-C_2POC_{12} is quite similar to that of *o*-C_3POC_{12}, as shown in Figure 12B. From the above discussion, we can see that the structure of the dye surfactants is of crucial importance in determining the final products directed by the mixed-surfactant system.

Possible Mechanism and Hypothesis for MCM-48 Formation. Room-temperature synthesis of MCM-48 is rarely reported. CTAB surfactant alone can only form a two-dimensional hexagonal mesophase in a surfactant−water binary system at room temperature. With the addition of a large amount of ethanol, MCM-48 can be formed at room temperature.[49] It was suggested that ethanol increases the surfactant packing parameter (*g*) and redirects the mesostructure form of hexagonal MCM-41 to cubic MCM-48. The surfactant packing parameter "*g*" is defined as $g = V/(a_0 l)$, where *V* is the total volume of surfactant chains plus any cosolvent organic molecule between chains, a_0 is the effective headgroup area at the micelle surface, and *l* is the kinetic surfactant tail length or the curvature elastic energy. This *g* factor originates from geometric constraints in the self-assembly of hydrocarbon amphiphiles. Small *g* values favor more curved surfaces, such as MCM-41 ($1/3 < g < 1/2$), while large *g* values favor structures with less curvature, such as MCM-48 ($1/2 < g < 2/3$) and layers ($g = 1$).[28] Liu et al. later systematically studied the effects of alcohol concentration on the structure of the mesoporous silica.[48] They proved that the mesoporous silica transformed from MCM-41 to MCM-48 and to lamellar phase by increasing the alcohol concentration. They also found that the amount of alcohol needed for obtaining a similar new phase increases with the decreasing chain length of the alcohol. This result is reasonable considering the fact that the hydrophobic nature of the alcohol increases with the increasing alkyl length. The more hydrophobic the nature of the alcohol, the higher amounts of alcohol located inside the micelles, and, as a result, a new phase with lower curvature is acquired easier. Gemini surfactants $C_{16-12-12-16}$ ($CH_3(CH_2)_{15}$-$(CH_3)_2N^+$ $(CH_2)_{12}N^+(CH_3)_2(CH_2)_{15}CH_3$) and $C_{22-12-22}$ (CH_3-$(CH_2)_{21}(CH_3)_2N^+$ $(CH_2)_{12}N+(CH_3)_2(CH_2)_{21}CH_3$) were found to favor the formation of MCM-48, even at room temperature.[28] It was thought that this may be due to similarity between the

SCHEME 2. Proposed Mechanism of the Formation of MCM-48 with Different Hemicyanine Dyes and CTAB Mixed Surfactants[a]

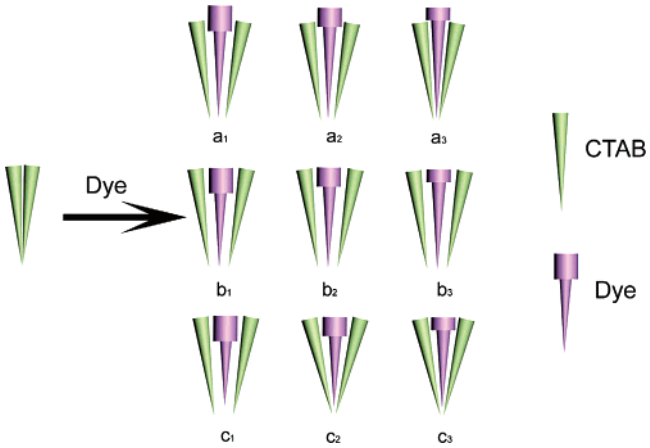

[a] The labels (a_1, a_2, etc.) correspond to the dyes labeled in Scheme 1.

micelle structures of $C_{16-12-12-16}$, $C_{22-12-22}$, and the CTAB−polar-additive−water system. These examples of synthesizing MCM-48 at room temperature can all be explained by the cosurfactant effect of the polar additives.

Because of the amphiphilic and rigid properties of the hemicyanine dye, the interactions between the dye molecules and the CTAB micelles are different from those between the organic additives and surfactant micelles. Mishra et al. studied the hemicyanine-dye−surfactant interaction and found that the hydrophobic chain of the dye molecules plays an important role in their action with CTAB surfactant.[50] It is proposed that mixed micelles are formed between amphiphilic hemicyanine dyes and CTAB surfactants, and the two aromatic rings normally present in hemicyanine dye are tightly associated with the CTAB positive headgroups, while the long hydrophobic tails are inserted into the micelle cores.[51] From the phase transformation behavior of the mesostructured silica, it can be seen that the phase behaviors of the mixed surfactant are influenced by both the hydrophilic headgroup size and the length of the long hydrophobic paraffin chain. We therefore propose a simplified scheme to help visualize the possible formation mechanism of MCM-48 at room temperature from the binary surfactant mixtures (Scheme 2). The formation of mixed micelles between CTAB molecules and dye molecules is dominated by the compatibility between the hydrophobic chain lengths of the two kinds of molecule. In the present case, the hydrophobic chain length of CTAB is fixed; therefore, this compatibility is determined by the effective chain length of the added hemicyanine dye molecules. As far as *o*-C_nPOC_{16} is concerned (Scheme 2), the effective hydrophobic chain length is a little bit longer than that of CTAB. As a result, only longer side-chain alkyls (linked to the pyridyl ring) such as butyl and propyl can penetrate effectively into the palisade region of the micelles. Consequently, only *o*-C_4POC_{16} and *o*-C_3POC_{16} are effective for the proper tuning of the packing parameter g ($1/2 < g < 2/3$) for the synthesis of MCM-48. When it comes to *o*-C_nPOC_{14} (Scheme 2), the effective hydrophobic/hydrophilic compatibility reaches its maximum, the short side-chain moieties can all effectively penetrate into the palisade region of the micelles, and MCM-48 can be formed effectively. For *o*-C_nPOC_{12} (Scheme 2), we propose that the shorter effective hydrophobic chain length makes it difficult to form mixed micelles with the CTAB surfactant, as can be deduced from the phase-transition behavior of the mesostructured silica upon the addition of the dye molecules (Note that the (100) peak position does not change as the amount of *o*-C_nPOC_{12} varies). In Figure 12A, we can see that MCM-48 can only be formed in a much narrower range compared with that of *o*-C_4POC_{16} and *o*-C_4POC_{14}. For *o*-C_3POC_{12} and *o*-C_2POC_{12}, the addition of more dye surfactants leads to a phase separation between CTAB and the dye molecules and the degradation of the order of the resultant mesostructured materials. Further investigation on the mechanism would be very useful to understand the new surfactant systems efficient for the synthesis of high-quality MCM-48 at room temperature.

Conclusion

At room temperature, highly ordered MCM-48 is prepared using hemicyanine-dye−CTAB mixtures as the template, and the whole process is quite straightforward and reproducible. The dye−CTAB mixtures can be viewed as cationic−cationic mixed-surfactant systems, which are reported for the first time to obtain MCM-48 at room temperature. The obtained MCM-48 has excellent thermal stability, even upon calcination in air at 900 °C for 5 h. Because of the blocking of the TICT state and the good dispersion of the dye molecules into the CTAB aggregates, the fluorescence lifetimes of the dye molecules trapped in the mesostructured silica are much longer than those of dye molecules in chloroform solution, despite the high dye doping ratio. Eight other dye congeners are further employed to investigate the mixed-surfactant systems, and it is revealed that the phase-transition behaviors of the mesostructured silica upon the addition of dye molecules are greatly influenced by the hemicyanine dye geometry. Upon a suitable ratio of an alkyl group on a pyridinium ring and an alkyloxy on a phenyl ring, for example, dyes *o*-C_4POC_{16}, *o*-C_4POC_{14}, *o*-C_4POC_{12}, *o*-C_3POC_{16}, *o*-C_3POC_{14}, and *o*-C_2POC_{14}, can lead to the synthesis of MCM-48 at room temperature. More importantly, thanks to the multifunctional properties of the hemicyanine dyes, we anticipate that the dye-doped mesostructured silica may find applications in areas of novel optoelectronic nano- or microdevices, ultrasensitive chemical/biological membrane/fiber sensors, stage-of-the-art information storage media, and beyond.

Acknowledgment. This work was financially supported by NNSFC (20221101, 50372002, 20030001065, 200490210, and 20471004), The National Basic Research Program (973 program, 2006CB601103), and NHTRDP (90401028). We gratefully acknowledge Dongyuan Zhao (Fudan University) and Jianbin Huang (Peking University) for helpful discussions.

Supporting Information Available: Synthesis procedures for the *o*-C_nPOC_m dyes. This material is available free of charge via the Internet at http://pubs.acs.org.

References and Notes

(1) Kresge, C. T.; Leonowicz, M. E.; Roth, W. J.; Vartuli, J. C.; Beck, J. S. *Nature* **1992**, *359*, 710.

(2) Beck, J. S.; Vartuli, J. C.; Roth, W. J.; Leonowicz, M. E.; Kresge, C. T.; Schmitt, K. D.; Chu, C. T. W.; Olson, D. H.; Sheppard, E. W.; McCullen, S. B.; Higgins, J. B.; Schlenker, J. L. *J. Am. Chem. Soc.* **1992**, *114*, 10384.

(3) Ying, J. Y.; Mehnert, C. P.; Wong, M. S. *Angew. Chem., Int. Ed.* **1999**, *38*, 56.

(4) Corma, A. *Top. Catal.* **1997**, *4*, 429.

(5) Mal, N. K.; Fujiwara, M.; Tanaka, Y. *Nature* **2003**, *421*, 350.

(6) Scott, B. J.; Wirnsberger, G.; Stucky, G. D. *Chem. Mater.* **2001**, *13*, 3140.

(7) Cavallaro, G.; Pierro, P.; Palumbo, F. S.; Testa, F.; Pasqua, L.; Aiello, R. *Drug Delivery* **2004**, *11*, 41.

(8) Schüth, F. *Chem. Mater.* **2001**, *13*, 3184.

(9) Schmidt, W.; Schüth, F. *Adv. Mater.* **2002**, *14*, 629.
(10) Stein, A. *Adv. Mater.* **2003**, *15*, 763.
(11) Taguchi, A.; Schüth, F. *Microporous Mesoporous Mater.* **2004**, *77*, 1.
(12) Huo. Q. S.; Margolese, D. I.; Ciesla, U.; Feng, P. Y.; Gier, T. E.; Sieger, P.; Leon. R.; Petroff, P. M.; Schüth, F.; Stucky, G. D. *Nature* **1994**, *368*, 317.
(13) Che, S.; Garcia-Bennett, A. E.; Yokoi, T.; Sakamoto, K.; Kunieda, H.; Terasaki, O.; Tatsumi, T. *Nat. Mater.* **2003**, *2*, 801.
(14) Che, S.; Liu, Z.; Ohsuna, T.; Sakamoto, K.; Terasaki, O.; Tatsumi, T. *Nature* **2004**, *429*, 281.
(15) Garcia-Bennett, A. E.; Terasaki, O.; Che, S.; Tatsumi, T. *Chem. Mater.* **2004**, *16*, 813.
(16) Tanev, P. T.; Pinnavavia, T. J. *Science* **1995**, *267*, 865.
(17) Bagshaw, S. A.; Prouzet, E.; Pinnavavia, T. J. *Science* **1995**, *269*, 1242.
(18) Huo. Q. S.; Leon, R.; Petroff, P. M.; Stucky, G. D. *Science* **1995**, *268*, 1324.
(19) Han, S. H.; Xu, J.; Hou, W. G.; Yu, X. M.; Wang, Y. S. *J. Phys. Chem. B.* **2004**, *108*, 15043.
(20) Zhao, D. Y.; Feng, J. L.; Huo, Q. S.; Melosh, N.; Fredrickson, G. H.; Chemlka, B. F.; Stuky, G. D. *Science* **1998**, *279*, 548.
(21) Zhao, D. Y.; Huo, Q. S.; Feng, J. L.; Chemlka, B. F.; Stuky, G. D. *J. Am. Chem. Soc.* **1998**, *120*, 6024.
(22) Monnier, A.; Schüth, F.; Huo, Q. S.; Kumar, D.; Margolese, D.; Maxwell, R. S.; Stuky, G. D.; Krishnamury, M.; Petroff, P.; Firouzi, A.; Janicke, M.; Chemlka, B. F. *Science* **1993**, *261*, 1299.
(23) Alderson, V.; Alderson, M. W. *Chem. Mater.* **1996**, *8*, 1141.
(24) Xu, J.; Luan, Z.; He, H.; Zhou, W.; Kevan, L. *Chem. Mater.* **1998**, *10*, 3690.
(25) Schmidt, R.; Junggreen, H.; Stocker, M. *Chem. Commun.* **1996**, 875.
(26) Gallis, K. W.; Laundry, Ch. C. *Chem. Mater.* **1997**, *9*, 2035.
(27) Van der Voort, P.; Morey, M.; Stucky, G. D.; Mathieu, M.; Vansant, E. F. *J. Phys. Chem. B.* **1998**, *102*, 585.
(28) Huo, Q. S.; Margolese, D.; Stuky, G. D. *Chem. Mater.* **1996**, *8*, 1147.
(29) Sayari, A. *J. Am. Chem. Soc.* **2000**, *122*, 6504.
(30) Liu, Y.; Karkamkar, A.; Pinnavavia, T. J. *Chem. Commun.* **2001**, 1822.
(31) Holland, P. M.; Rubingh, D. N. In *Mixed Surfactant Systems*; Holland, P. M., Rubingh, D. N., Eds.; ACS Symposium Series 501; American Chemical Society: Washington, DC, 1992; pp 2−30.
(32) Ryoo, R.; Joo, S. H.; Kim, J. M. *J. Phys. Chem. B.* **1998**, *103*, 7435.
(33) Kruk, M.; Jaroniec, M.; Ryoo, R.; Joo, S. H. *Chem. Mater.* **2000**, *12*, 1414.
(34) Chen, F. X.; Huang, L. M.; Li, Q. Z. *Chem. Mater.* **1997**, *9*, 2685.
(35) Abraham, U. *An Introduction to Ultrathin Organic Films: From Langmuir−Blodgett to Self-Assembly*; Academic Press: Boston, MA, 1991.
(36) He, G. S.; Bhawalkar, J. D.; Zhao, C. F.; Prasad, P. N. *Appl. Phys. Lett.* **1995**, *67*, 2433.
(37) Jones, M. A.; Bohn, P. W. *Anal. Chem.* **2000**, *72*, 3776 and references therein.
(38) Wang, Z. S.; Li, F. Y.; Huang, C. H.; Wang, L.; Wei, M.; Jin, L. P.; Li, N. Q. *J. Phys. Chem. B.* **2000**, *104*, 9676.
(39) Stathatos, E.; Lianos, P.; Laschewsky, A.; Ouari, O.; Van Cleuvenbergen, P. *Chem. Mater.* **2001**, *13*, 3888.
(40) Hou, K.; Shen, L.; Huang, C. Unpublished results, 2005.
(41) (a) Heike, L.; Peter, C.; Urlich-W, G. *J. Prakt. Chem./Chem.-Ztg.* **1994**, *336*, 521. (b) Hassner, A.; Birnbaum, D.; Loew, L. M. *J. Org. Chem.* **1984**, *49*, 2546.
(42) Cassiers, K.; Linssen, T.; Mathieu, M.; Benjelloun, M.; Schrijnemakers, K.; Van der Voort, P.; Cool, P.; Vansant, E. F. *Chem. Mater.* **2002**, *14*, 2317.
(43) Pang, J. B.; Hampsey, J. E.; Hu, Q. Y.; Wu, Z. W.; John, V. T.; Lu, Y. F. *Chem. Commun.* **2004**, 682.
(44) Chen, C. Y.; Li, H. X.; Davis, M. E. *Microporous Mater.* **1993**, *2*, 17. (b) Romero, A. A.; Alba, M. D.; Klinowski, J. *J. Phys. Chem. B* **1998**, *102*, 123.
(45) Honma, I.; Zhou, H. S. *Chem. Mater.* **1998**, *10*, 103.
(46) Kim, J.; Lee, M. *J. Phys. Chem. A* **1999**, *103*, 3378 and references there in.
(47) Pakatchi, M.; Lal, S.; He, G. S.; Kim, K. S.; Prasad, P. N. *Chem. Mater.* **1999**, *11*, 3012.
(48) Liu, S. Q.; Cool, P.; Collart, O.; Van der Voort, P.; Vansant, E. F.; Lebedev, O. I.; Van Tendeloo, G.; Jiang, M. H. *J. Phys. Chem. B.* **2003**, *107*, 10405.
(49) Schumacher, K.; Grun, M.; Unger, K. K. *Microporous Mesoporous Mater.* **1999**, *27*, 201.
(50) Mishra, M.; Patel, S.; Behera, R. K.; Mishra, B. K.; Behera, G. B. *Bull. Chem. Soc. Jpn.* **1997**, *70*, 2913.
(51) Bunton, C. A.; Minch, M. J.; Hidalyo, J., Sepulveda, L. J. *J. Am. Chem. Soc.* **1973**, *95*, 3262.